Published in final edited form as:
IEEE Trans Biomed Eng. 2011 August ; 58(8): . doi:10.1109/TBME.2011.2153851.

Measurement of strain and strain rate in embryonic chick heart in vivo using spectral domain optical coherence tomography

Peng Li,
Department of Bioengineering, University of Washington, Seattle, WA 98195, USA

Xin Yin,
Department of Biomedical Engineering, Oregon Health & Science University, Portland, OR 97239, USA

Liang Shi,
Department of Biomedical Engineering, Oregon Health & Science University, Portland, OR 97239, USA

Aiping Liu,
Department of Biomedical Engineering, Oregon Health & Science University, Portland, OR 97239, USA

Sandra Rugonyi, and
Department of Biomedical Engineering, Oregon Health & Science University, Portland, OR 97239, USA

Ruikang K Wang
Department of Bioengineering, University of Washington, Seattle, WA 98195, USA

Ruikang K Wang: wangrk@uw.edu

Abstract

The ability to measure *in vivo* strain and strain rate in embryonic chick heart is one of the key requirements for understanding the mechanisms of cardiac development. Due to its high temporal and spatial resolution as well as its fast imaging capability, optical coherence tomography (OCT) has the potential to reveal the complex myocardial activity in the living chick heart. We describe a method to evaluate the *in vivo* strain and strain rate of the myocardium through analyzing the periodic variation of the myocardial wall thickness calculated from real time serial OCT images. The results demonstrate that OCT can be a useful tool to describe the biomechanical characteristics of the embryonic heart.

Index Terms

Optical coherence tomography; Medical and biological imaging; Cardiac development; Myocardial strain; Embryonic chick heart

I. Introduction

Cardiac development depends on a dynamic interaction of genetic and environmental factors [1–4]. During the process, the genes determine the generation of the basic elements, such as cells, extracellular matrix, adhesion molecules, and how these basic elements are assembled

Correspondence to: Ruikang K Wang, wangrk@uw.edu.

into a properly functional heart. However, this process is also modulated and influenced by the local biomechanical environment to which cardiac cells are exposed. Thus, in order to fully understand the mechanisms of cardiac development, it is necessary to know the mechanical characteristics of the embryonic heart.

Usually, stress and strain are employed to quantitatively outline the biomechanical environment. Correspondingly, a number of technologies have been developed to measure them in the embryonic heart. The wall shear stress can be determined by calculating velocity gradients of blood flow in a direction perpendicular to the wall [5, 6]. Wall stress, however, is difficult to measure directly, and is frequently estimated using measured intracardiac pressure and cardiac wall thickness [7]. Comparatively speaking, the myocardial wall strain can be determined reliably from images. Once the strain is known, stress can be studied via strain-stress relationships.

In order to study how the epicardial strains vary with heart development, Taber *et al.* measured ventricular (surface) strains in embryonic chicks from stage HH16 to HH24 by tracking the motion of microsphere triangular arrays that were placed on the myocardial surface in the embryonic heart [8]. Similar methods were employed to study the developmental and functional mechanisms during looping by determining the regional myocardial wall strains in embryonic chick [9, 10]. In a later work, optical coherence tomography was used to obtain the three-dimensional (3D) structure of embryonic chick heart, from which the positions of marker-arrays were tracked [10]. In a mature heart, 3D myocardial wall strain can be determined by tracking the motion of myocardial markers [11–13]. However, as to the embryonic heart, only the 2D myocardial strains can be obtained by this kind of method, and it is impossible to obtain the radial strain (wall thickening and thinning) due to small dimensions of the developing myocardial wall.

The myocardial wall deformation can also be calculated by means of 3D imaging [14–16]. However, in the past, there was no imaging technique available that could provide real-time *in vivo* visualization of the internal microstructure and its associated dynamic motion in the embryonic chick heart at high resolution. Magnetic resonance imaging is currently not capable of real-time imaging. Ultrasound techniques can realize real-time acquisition in the mature heart [15, 16], but it is difficult, if not impossible, to be applied to the early embryonic heart mostly due to its relatively low spatial resolution. Additionally, confocal microscopy provides high resolution images, but it cannot penetrate the entire embryonic chick heart.

Optical coherence tomography (OCT) is a powerful, noninvasive imaging technique with high temporal and spatial resolution with an imaging depth of up to 2 mm in highly scattering biological tissue [17, 18]. This attribute makes OCT uniquely suited for the study of the embryonic heart at its early developmental stages [5, 10, 19–25]. OCT has been demonstrated in a number of embryonic models, such as Rana pipiens tadpole [26], Xenopus laevis [27], zebrafish [28], chick [20, 29], and mouse [30, 31]. Briefly, the OCT imaging of the embryonic heart can be classified into two categories: 1) morphological imaging: due to the constant improvement of OCT system imaging speed over the time, it has been evolved from the 2D cross sectional imaging [20, 26, 27] to 3D [29–31] and even 4D (3D volume over time) volumetric imaging [23, 24, 32] to better understand the morphological dynamics; 2) functional imaging: as an extension of OCT, Doppler OCT enables the hemodynamic study in embryonic heart [5, 19, 22, 31, 33, 34], such as monitoring of the blood flow velocity [5, 21, 31], shear rate [22], and shear stress [33, 34].

In this study, we describe a method to measure *in vivo* the radial strain of the myocardial wall in the early embryonic chick heart using spectral domain OCT technology. Specifically,

because of its high imaging speed, we demonstrate that OCT is able to resolve the motion of the myocardial wall as a function of time. The high spatial resolution of OCT enables us to calculate the dynamic variation of the wall thickness with high precision by tracing the borders of myocardial wall from serial OCT images, from which the radial velocity, radial strain and strain rate of myocardial wall are deduced.

II. Material and Methods

A. Chick Embryo Preparation

Following standard procedures of embryo preparation [35–37], fertilized white Leghorn chick eggs were incubated blunt-end up at 38 °C and 85% humidity in a horizontal rotation incubator to the desired developmental stage, HH18, which is about 3 days of incubation following Hamburger-Hamilton staging [38]. At this early stage of development, the chick heart is tubular and has no valves; the outflow tract (OFT) is the distal region of the embryonic heart—connecting the ventricle with the arterial system—and functions as a primitive valve by contracting to limit blood flow regurgitation. The OFT is a crucial cardiac segment subjected to numerous studies because a large portion of congenital heart defects originate in the OFT [39].

To expose the embryonic heart, the egg shell was opened at the air sac end, and a small section of the inner shell membrane was carefully removed. Then the egg was placed into the OCT sample arm for *in vivo* imaging, with the probing light access from the top. In order to maintain a constant temperature of 37.5°C during the data acquisition, a home-built organic glass box equipped with a heating blanket was used to house the egg under the sample arm. The constant temperature control in the housing box was achieved by an automatic feedback system that employed a small thermocouple, placed near the embryo, to provide the control of the temperature of the heating blanket in real time.

B. OCT System Setup

All experiments were performed on an OCT system (see Fig. 1), specifically designed for chick embryo imaging. The system was based on a spectral domain configuration, employing a fast InGaAs line scan camera operating at a 47 kHz A-scan rate. In the system, a broadband superluminescent diode (SLD) (central wavelength λ_0=1321.5 nm, bandwidth $\Delta\lambda$=52 nm) was used as the low-coherent light source, yielding ~14 μm axial resolution in air. The emitted radiation from SLD was coupled into a fiber-based Michelson interferometer via a broadband optical circulator. In the sample arm, the light was focused onto the sample by an objective lens (focal length f=50 mm), providing a measured lateral resolution at ~16 μm. And the probe beam scanning was realized by an X-Y galvanometer scanner in this arm. The interference signal was routed into a home-built spectrometer via the optical circulator. The spectrometer had a designed spectral resolution of ~0.088 nm, providing a detectable depth range of ~4.6 mm. With these configurations, the signal to noise ratio of the system was measured at ~105 dB with a light power of ~3 mW on the sample.

The B scan, i.e., X direction scan, was achieved by the X-scanner driven with a saw tooth function. During one lateral B-scan cycle, 256 axial A-lines were acquired to cover ~1.1 mm on the chick embryo heart. The overlap between adjacent two A-scans was about 75% (lateral diameter of sampling light focus point was ~16 um). With the camera running at 47 kHz A-scan rate, the acquisition rate for B-scan frames was 140 frames per second (fps). 200 repeated B-scans were acquired as the M-scan, i.e. M-B scan mode, covering 3–4 cardiac periods of the beating heart, from which the velocity, strain and strain rate of the myocardium were calculated.

C. Image Analysis

With the OCT imaging as described above, 200 sequential 2D cross-sectional images at the same location, i.e., M-B scans representing a 3D data cube, were acquired from the beating embryonic chick heart, from which the myocardium was identified. In order to better illustrate the motion of the myocardial wall during each cardiac beat, M-mode images at the selected lines passing through the center of the lumen were used to evaluate the dynamic wall thickness via post-processing of the M-B scan dataset. As we know, the cardiac jelly is a layer of extracellular matrix unevenly distributed between the lumen and myocardium, and the lumen has a slit-shaped cross-section when the OFT is most contracted [20]. Thus, we used the slit-shaped cross-section as a reference to extract the M-mode images at the selected lines from the 3D data cube. In order to consider the influence of the cardiac jelly on the deformation of the myocardial wall, we investigated the M-mode images along two distinct lines (1 and 2) passing through the center of the lumen, respectively, one oriented at the position nearly parallel to and the other perpendicular to the slit-shaped lumen when the OFT is most contracted. This treatment ensures that the velocity, strain and strain rate calculated (see below) represent the radial wall motion.

To extract the wall thickness from the M-mode images, we developed a semi-automatic program in MATLAB. The flow chart of the program is illustrated in Fig. 2. First, the myocardial wall border lines in the M-mode structural images were found. The program then required a user to manually select several points as the seeds along the myocardial wall, and then interpolate between these points to give the whole border trace [40]. Once the outer and inner borders of myocardial wall were obtained, the myocardial wall thickness and mean radial velocity versus time can be determined via a subtraction and gradient operation, respectively. It should be noted that the mean radial velocity discussed here is half the sum of the radial velocities of outer and inner borders. In order to reduce the errors due to the manual selection of the seeding points and the drift of OFT over time during the acquisition of dataset (because of the pulsed blood flow), the border extraction procedure was repeated 8 times for averaging.

The deformation of myocardial wall is quantified using the natural strain, $\varepsilon(t)$ [41]. Here, we focused on the radial component of strain and strain rate, thus only the change of wall thickness T needs to be calculated. If dt denotes an infinitesimal time interval, then $d\varepsilon(t)$ can be defined as the infinitesimal amount of change in thickness during this time interval, relative to the thickness at a previous time instance:

$$d\varepsilon(t)=\frac{T(t+dt)-T(t)}{T(t)}, \quad (1)$$

where $T(t)$ is the wall thickness at the time t. The total amount of natural strain $\varepsilon(t)$ over the time t can then be obtained by integrating $d\varepsilon(t)$:

$$\varepsilon(t)=\int_{t_0}^{t} d\varepsilon(t). \quad (2)$$

According to Eqs. (1) and (2), the calculated natural strain values should be zero at the time t_0 and at the time instants when the wall has the same thickness as at the time t_0. This kind of result might give the impression that the wall shape at time t_0 was considered as its original shape. However, because the heart muscle returns to its original shape at the phase when OFT is most expanded, it is usually assumed that the strain value at this time instant is zero [8, 9]. During imaging, it is difficult to ascertain that the beginning time t_0 is exactly at the time when OFT is most expanded. Thus, a constant compensation is required to make the strain at the OFT most expanded phase to return to zero.

Strain rate ε' is defined as the speed at which the strain occurs [41]. For the myocardial thickness, it can be written as:

$$\varepsilon'(t)=\frac{T'(t)}{T(t)}, \quad (3)$$

where $T'(t)$ is the rate of change of thickness, which can be obtained via a gradient operation with respect to the time t.

III. Results and Discussion

The cross section of the embryonic chick OFT and M-mode structural images along lines 1 and 2 are shown in Fig. 3. The microstructures within the OFT wall, e.g., OFT lumen, cardiac jelly and myocardium, can be distinctly identified from the cross-sectional images (Fig. 3a). When the OFT is most contracted, lumen has a slit-shaped cross-section. The cardiac jelly has an uneven distribution, which may result from the requirement that the developing heart needs to optimize the mechanical efficiency of peristaltic blood pump [20]. The myocardium is the outmost layer of the OFT, which actively contracts. As illustrated in Figs. 3b and 3c, the M-mode images clearly revealed the periodic variation of the myocardial thickness as a function of time during the cardiac cycle. We find that the two walls, either in Fig. 3b (above and beneath the lumen) or in Fig. 3c (right and left of the lumen), expand and extract at the same time, thus it is reasonable to assume that this cross-section is almost perpendicular to the myocardial wall.

From Fig. 4, it is seen that the myocardial outer and inner borders were respectively extracted with the program described above. However, the absorption of the blood strongly attenuates the OCT signal, making it difficult to extract the borders beneath the lumen (see Fig. 4a). However, we find that the motion of the two walls, either in Fig. 4a or in Fig. 4b, have no significant difference. For this reason, we just selected one of the two walls for each case to calculate the strain and strain rate.

The strain and strain rate of the myocardial wall were plotted versus time in Fig. 5. The myocardial wall thickness and mean radial velocity (i.e. the velocity at which the myocardium expands and contract in the radial direction) were also included in the figure. Note that the extracted myocardial wall thickness was normalized according to its maximum value (Fig. 5a). It was found that all these curves vary periodically with time. In addition, for each parameter, the curves along the line 1 and line 2 have a similar trend.

As shown in the mean velocity curves (Fig. 5b), the intersection points between the curves and the lines marked at ‘velocity=0’ point out the time when the OFT is most contracted or expanded. A small phase shift (time delay) between the two curves, i.e., evaluated from lines 1 and 2, respectively, was found. This phase shift might appear because the imaged cross-section might not be perpendicular to the wall. Also, image noise and errors in the tracing of wall motions might contribute to this phase lag.

As to the strain calculation (Fig. 5c), although the natural strain along line 2 seems a little lower than the strain along line 1, this is within the errors introduced by image noise and the tracing method, and thus we may conclude that the myocardial wall deformations along the two lines show the same scale. However, their deformations are not at the same rhythm, as shown in the strain rate calculation (Fig. 5d). Most likely due to the movement of jelly, the valley of strain curve along the line 2 sometimes does not locate at the time when OFT is most expanded.

Because of the lack of related published data about the radial strain (wall thickening and thinning) and strain rate of HH18 chick OFT, it is difficult for us to compare our results with the other approaches. Taber *et al.* reported that the primitive right ventricle of HH18 chick has a circumferential strain 10%–15% and longitudinal strain 15%–20% at the end-diastole [8]. Additionally, Fleming *et al.* reported the highest strain rate 5–10 s^{-1} for the mature left-ventricle posterior wall during the cardiac beat by color Doppler imaging [42]. To our knowledge, no other work reported radial strains in the chick developing heart.

With the OCT M-mode structural imaging technique, physical parameters, such as mean radial velocity, radial strain and strain rate, of the myocardial wall were extracted. However, the technique requires the image segmentation to trace the borders of the myocardial wall, and the border extraction is mainly based on the magnitude signal of OCT, which is inevitably influenced by the OCT system noise and spatial resolution. In order to determine the strain rate via the temporal gradient operation, which is very sensitive to noise, considerable attention should be paid to make the trace as smooth as possible. Further effort is needed in this regard, to improve the accuracy of the technique by suppressing the noise and segmentation errors.

It was found that the M-mode structural imaging technique actually characterizes the axial deformation of the myocardial wall, which is the component along the probing light axis. Thus the estimated values of myocardial wall deformation are angle dependent. In order to get the radial component, effort should be paid to make the probing light perpendicular to the myocardial wall during the acquisition of the datasets. This process is also user-dependent. Fortunately, although the amplitude of the deformation is influenced by the direction of probing light, it does not have a significant impact on the profiles of the strain curves, provided that the angle between the direction of probing light and radial direction of wall deformation does not change greatly during the imaging.

In the current study, only the radial deformation (wall thickening and thinning) is estimated by the M-mode structural imaging technique. However, it serves as an important complement to the 2D surface deformation measurement by tracking the motion of microsphere triangular arrays [8–10]. In fact, this technique has the potential to determine all the three components of deformation, namely radial, longitudinal and circumferential component, by 4D (3D volumetric data + time) imaging technique. In our future work, we plan to calculate the tangent plane of the myocardium from the 4D datasets, upon which the angle between the probe beam direction and the axis of three deformation components will be deduced to obtain the 3D deformation characteristics of the beating embryonic chick heart. Because there exists a relation between stress and strain, once the 3D deformation is known, it may be possible to provide a means to characterize the stress of the myocardial wall, and thus more completely characterize the biomechanical environment.

IV. Conclusion

The strain and strain rate measurement of embryonic chick heart is a meaningful approach in the investigations of cardiac development. In this study, we have presented a method to measure *in vivo* the strain and strain rate of myocardial wall that occurs in the embryonic chick heart during each cardiac beat by using the high resolution and high speed OCT as an enabling tool. To our knowledge, this is the first time that the radial strain in embryonic chick heart was measured *in vivo*. This ability would represent a significant complement to the 2D surface strain measurement for further understanding the mechanical characteristics of the primitive heart. Furthermore, the OCT imaging technique has the potential to be extended to 3D strain and strain rate measurements.

Acknowledgments

This work was supported in part by an NIH grant, R01HL094570, from the National Heart, Blood and Lung Institute.

References

1. Clark EB, Hu N, Frommelt P, Vandekieft GK, Dummett JL, Tomanek RJ. Effect of increased pressure on ventricular growth in stage 21 chick embryos. Am J Physiol. 1989; 257:H55–61. [PubMed: 2750949]
2. Fishman MC, Stainier DY. Cardiovascular development. Prospects for a genetic approach. Circ Res. 1994; 74:757–763. [PubMed: 8156624]
3. Groenendijk BC, Hierck BP, Vrolijk J, Baiker M, Pourquie MJ, Gittenberger-de Groot AC, Poelmann RE. Changes in shear stress-related gene expression after experimentally altered venous return in the chicken embryo. Circ Res. 2005; 96:1291–1298. [PubMed: 15920020]
4. Hove JR, Koster RW, Forouhar AS, Acevedo-Bolton G, Fraser SE, Gharib M. Intracardiac fluid forces are an essential epigenetic factor for embryonic cardiogenesis. Nature. 2003; 421:172–177. [PubMed: 12520305]
5. Ma Z, Liu A, Yin X, Troyer A, Thornburg K, Wang RK, Rugonyi S. Measurement of absolute blood flow velocity in outflow tract of HH18 chicken embryo based on 4D reconstruction using spectral domain optical coherence tomography. Biomed Opt Express. 2010; 1:798–811. [PubMed: 21127734]
6. Poelma C, Van der Heiden K, Hierck BP, Poelmann RE, Westerweel J. Measurements of the wall shear stress distribution in the outflow tract of an embryonic chicken heart. J R Soc Interface. 2010; 7:91–103. [PubMed: 19401309]
7. Miller CE, Wong CL, Sedmera D. Pressure overload alters stress-strain properties of the developing chick heart. Am J Physiol Heart Circ Physiol. 2003; 285:H1849–1856. [PubMed: 12855423]
8. Taber L, Sun H, Clark E, Keller B. Epicardial strains in embryonic chick ventricle at stages 16 through 24. Circ Res. 1994; 75:896–903. [PubMed: 7923636]
9. Alford PW, Taber LA. Regional epicardial strain in the embryonic chick heart during the early looping stages. J Biomech. 2003; 36:1135–1141. [PubMed: 12831739]
10. Filas BA, Efimov IR, Taber LA. Optical coherence tomography as a tool for measuring morphogenetic deformation of the looping heart. Anat Rec (Hoboken). 2007; 290:1057–1068. [PubMed: 17721979]
11. Waldman LK, Fung YC, Covell JW. Transmural myocardial deformation in the canine left ventricle. Normal in vivo three-dimensional finite strains. Circ Res. 1985; 57:152–163. [PubMed: 4006099]
12. Waldman LK, Nosan D, Villarreal F, Covell JW. Relation between transmural deformation and local myofiber direction in canine left ventricle. Circ Res. 1988; 63:550–562. [PubMed: 3409487]
13. Villarreal FJ, Lew WY, Waldman LK, Covell JW. Transmural myocardial deformation in the ischemic canine left ventricle. Circ Res. 1991; 68:368–381. [PubMed: 1991344]
14. Rademakers FE, Bogaert J. Left ventricular myocardial tagging. Int J Card Imaging. 1997; 13:233–245. [PubMed: 9220285]
15. Guth B, Savage R, White F, Hagan A, Samtoy L, Bloor C. Detection of ischemic wall dysfunction: Comparison between M-mode echocardiography and sonomicrometry. American Heart Journal. 1984; 107:449–457. [PubMed: 6695687]
16. Sutherland GR, Stewart MJ, Groundstroem KW, Moran CM, Fleming A, Guell-Peris FJ, Riemersma RA, Fenn LN, Fox KA, McDicken WN. Color Doppler myocardial imaging: a new technique for the assessment of myocardial function. J Am Soc Echocardiogr. 1994; 7:441–458. [PubMed: 7986541]
17. Fercher AF. Optical coherence tomography - development, principles, applications. Z Med Phys. 2003; 20:251–276. [PubMed: 21134630]
18. Tomlins PH, Wang RK. Theory, developments and applications of optical coherence tomography. Journal of Physics D: Applied Physics. 2005; 38:2519.

19. Davis AM, Rothenberg FG, Shepherd N, Izatt JA. In vivo spectral domain optical coherence tomography volumetric imaging and spectral Doppler velocimetry of early stage embryonic chicken heart development. J Opt Soc Am A Opt Image Sci Vis. 2008; 25:3134–3143. [PubMed: 19037405]
20. Männer J, Thrane L, Norozi K, Yelbuz TM. High-resolution in vivo imaging of the cross-sectional deformations of contracting embryonic heart loops using optical coherence tomography. Developmental Dynamics. 2008; 237:953–961. [PubMed: 18330931]
21. Rugonyi S, Shaut C, Liu A, Thornburg K, Wang RK. Changes in wall motion and blood flow in the outflow tract of chick embryonic hearts observed with optical coherence tomography after outflow tract banding and vitelline-vein ligation. Phys Med Biol. 2008; 53:5077–5091. [PubMed: 18723935]
22. Davis A, Izatt J, Rothenberg F. Quantitative measurement of blood flow dynamics in embryonic vasculature using spectral Doppler velocimetry. Anat Rec (Hoboken). 2009; 292:311–319. [PubMed: 19248163]
23. Liu A, Wang R, Thornburg KL, Rugonyi S. Efficient postacquisition synchronization of 4-D nongated cardiac images obtained from optical coherence tomography: application to 4-D reconstruction of the chick embryonic heart. J Biomed Opt. 2009; 14:044020. [PubMed: 19725731]
24. Gargesha M, Jenkins MW, Wilson DL, Rollins AM. High temporal resolution OCT using image-based retrospective gating. Opt Express. 2009; 17:10786–10799. [PubMed: 19550478]
25. Bhat S, Larina IV, Larin KV, Dickinson ME, Liebling M. Multiple-cardiac-cycle noise reduction in dynamic optical coherence tomography of the embryonic heart and vasculature. Opt Lett. 2009; 34:3704–3706. [PubMed: 19953168]
26. Boppart SA, Brezinski ME, Bouma BE, Tearney GJ, Fujimoto JG. Investigation of developing embryonic morphology using optical coherence tomography. Dev Biol. 1996; 177:54–63. [PubMed: 8660876]
27. Boppart SA, Tearney GJ, Bouma BE, Southern JF, Brezinski ME, Fujimoto JG. Noninvasive assessment of the developing Xenopus cardiovascular system using optical coherence tomography. Proc Natl Acad Sci U S A. 1997; 94:4256–4261. [PubMed: 9113976]
28. Kagemann L, Ishikawa H, Zou J, Charukamnoetkanok P, Wollstein G, Townsend KA, Gabriele ML, Bahary N, Wei X, Fujimoto JG, Schuman JS. Repeated, noninvasive, high resolution spectral domain optical coherence tomography imaging of zebrafish embryos. Mol Vis. 2008; 14:2157–2170. [PubMed: 19052656]
29. Yelbuz TM, Choma MA, Thrane L, Kirby ML, Izatt JA. Optical coherence tomography: a new high-resolution imaging technology to study cardiac development in chick embryos. Circulation. 2002; 106:2771–2774. [PubMed: 12451001]
30. Luo W, Marks DL, Ralston TS, Boppart SA. Three-dimensional optical coherence tomography of the embryonic murine cardiovascular system. J Biomed Opt. 2006; 11:021014. [PubMed: 16674189]
31. Larina IV, Furushima K, Dickinson ME, Behringer RR, Larin KV. Live imaging of rat embryos with Doppler swept-source optical coherence tomography. J Biomed Opt. 2009; 14:050506. [PubMed: 19895102]
32. Jenkins MW, Adler DC, Gargesha M, Huber R, Rothenberg F, Belding J, Watanabe M, Wilson DL, Fujimoto JG, Rollins AM. Ultrahigh-speed optical coherence tomography imaging and visualization of the embryonic avian heart using a buffered Fourier Domain Mode Locked laser. Opt Express. 2007; 15:6251–6267. [PubMed: 19546930]
33. Jenkins MW, Peterson L, Gu S, Gargesha M, Wilson DL, Watanabe M, Rollins AM. Measuring hemodynamics in the developing heart tube with four-dimensional gated Doppler optical coherence tomography. J Biomed Opt. 2010; 15:066022. [PubMed: 21198196]
34. Liu A, Wang R, Thornburg K, Rugonyi S. Dynamic variation of hemodynamic shear stress on the walls of developing chick hearts: computational models of the heart outflow tract. Engineering with Computers. 2009; 25:73–86.

35. Clark EB, Rosenquist GC. Spectrum of cardiovascular anomalies following cardiac loop constriction in the chick embryo. Birth Defects Orig Artic Ser. 1978; 14:431–442. [PubMed: 737312]

36. Hu N, Connuck DM, Keller BB, Clark EB. Diastolic filling characteristics in the stage 12 to 27 chick embryo ventricle. Pediatr Res. 1991; 29:334–337. [PubMed: 1852525]

37. Keller BB, Hu N, Serrino PJ, Clark EB. Ventricular pressure-area loop characteristics in the stage 16 to 24 chick embryo. Circ Res. 1991; 68:226–231. [PubMed: 1984865]

38. Hamburger V, Hamilton HL. A series of normal stages in the development of the chick embryo. Journal of Morphology. 1951; 88:49–92.

39. Gittenberger-de Groot AC, Bartelings MM, Deruiter MC, Poelmann RE. Basics of cardiac development for the understanding of congenital heart malformations. Pediatr Res. 2005; 57:169–176. [PubMed: 15611355]

40. Fujimoto S, Oki T, Tabata T, Tanaka H, Yamada H, Oishi Y, Ishimoto T, Ito S, Abe Y, Kanda R. Novel approach to the quantitation of regional left ventricular systolic and diastolic function using tissue Doppler imaging to create a myocardial velocity profile and gradient. Circ J. 2003; 67:416–422. [PubMed: 12736480]

41. D'Hooge J, Heimdal A, Jamal F, Kukulski T, Bijnens B, Rademakers F, Hatle L, Suetens P, Sutherland GR. Regional strain and strain rate measurements by cardiac ultrasound: principles, implementation and limitations. Eur J Echocardiogr. 2000; 1:154–170. [PubMed: 11916589]

42. Fleming AD, Xia X, McDicken WN, Sutherland GR, Fenn L. Myocardial velocity gradients detected by Doppler imaging. Br J Radiol. 1994; 67:679–688. [PubMed: 8062010]

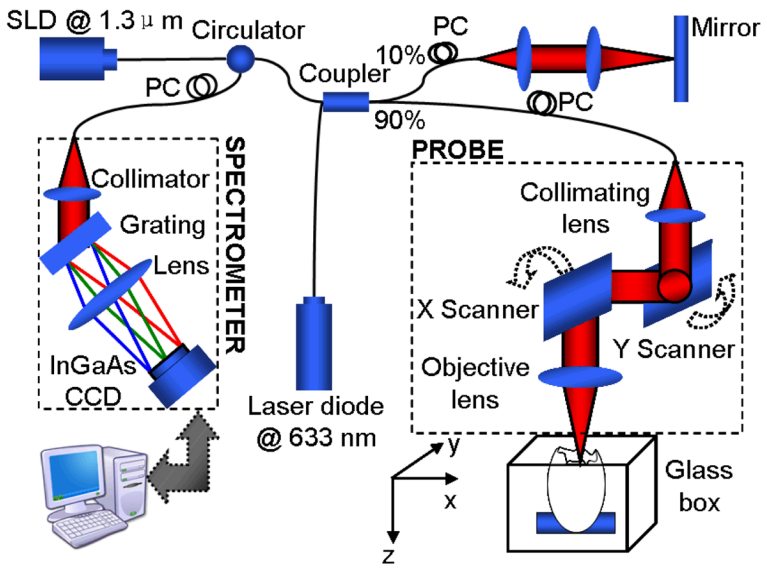

Fig. 1.
Schematic of a spectral-domain OCT system

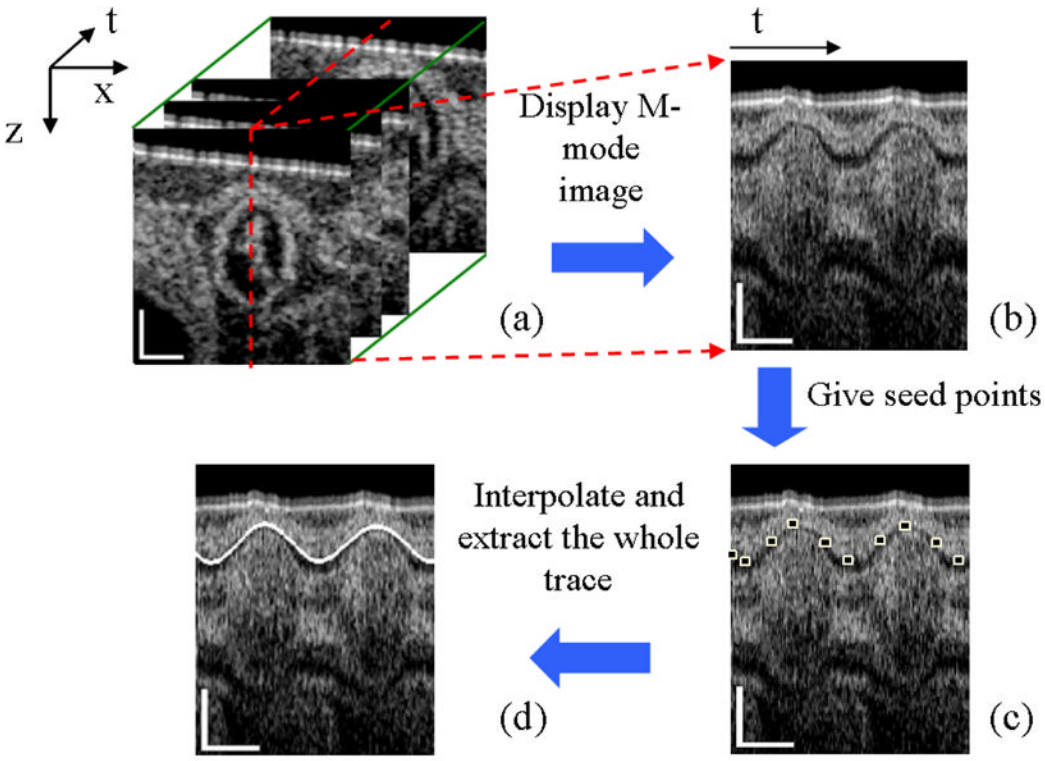

Fig. 2.

Flow chart of myocardial border extraction: Extract M-mode image (b) from M-B scan dataset (a) at the selected red line; Give several seed points as shown in (c); Interpolate between these points and give the whole trace (d). The scale bars in (a) and the vertical scale bars in (b) (c) and (d) represent 200μm; the lateral scale bars in (b) (c) and (d) represent 0.2s.

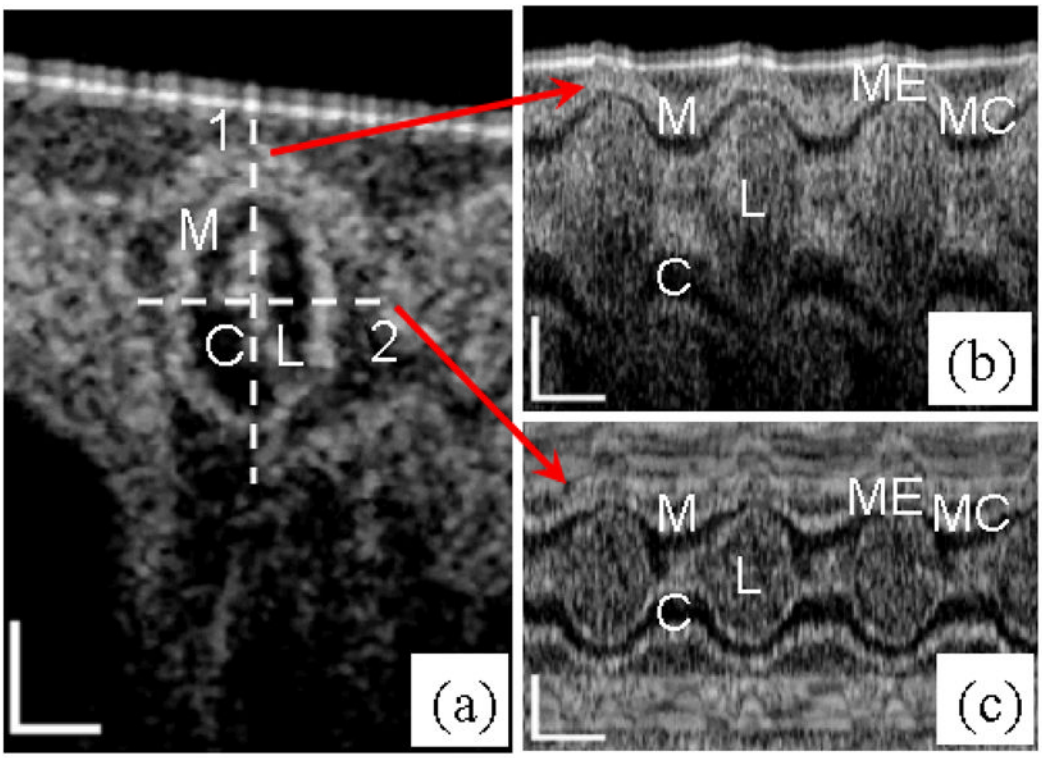

Fig. 3.

OCT images of HH18 chick OFT. Left: (a) Typical cross-sectional image when the OFT is most constricted. Right: M-mode images along the (b) line 1 and (c) line 2. M: myocardium; C: cardiac jelly; L: lumen; MC: OFT is most contracted; ME: OFT is most expanded. The scale bars in (a) and the vertical scale bars in (b) and (c) represent 200μm; the lateral scale bars in (b) and (c) represent 0.2s.

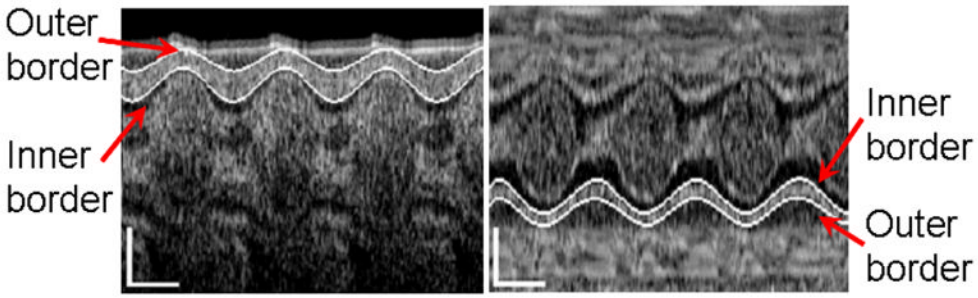

Fig. 4.

Extraction of myocardial border lines of embryonic chick heart along the (a) line 1 and (b) line 2. The vertical scale bars represent 200μm; the lateral scale bars represent 0.2s.

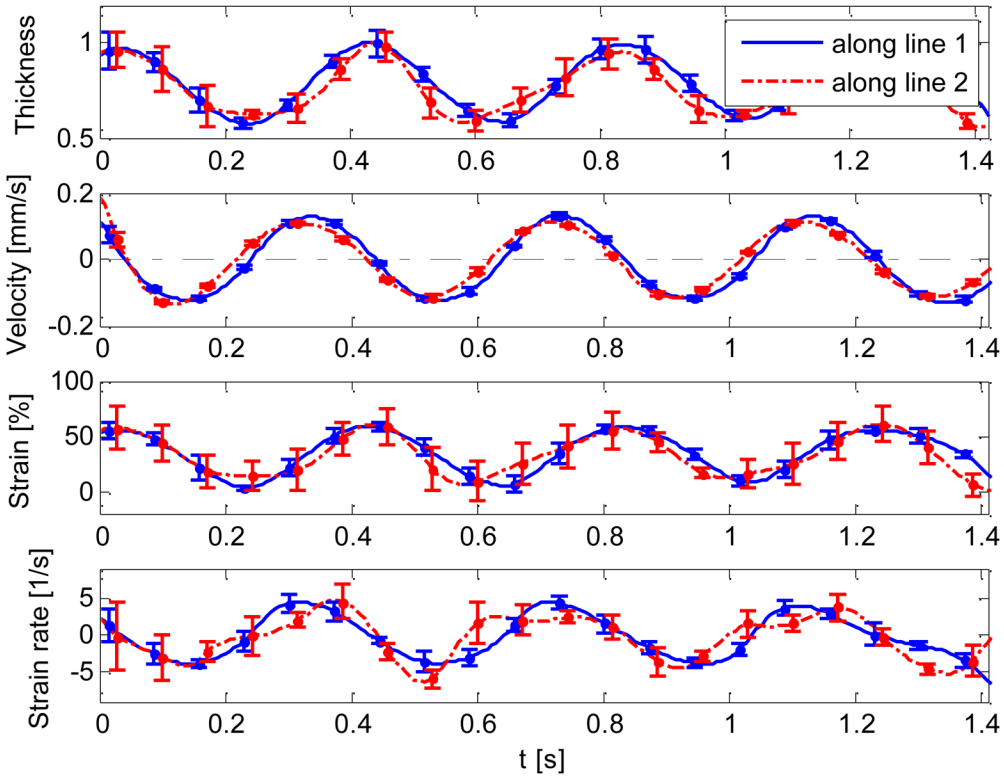

Fig. 5.
Normalized thickness, mean velocity, radial strain and strain rate of HH18 chick OFT extracted from the OCT M-mode imaging along the line 1 and line 2. The vertical dash-dot lines show the cardiac phases, E: expansion; C: contraction.